

PAPER • OPEN ACCESS

Dosimetric characterization of double network Fricke hydrogel based on PVA-GTA and phenylalanine peptide derivative




To cite this article: Salvatore Gallo *et al* 2024 *J. Phys. D: Appl. Phys.* **57** 075303

View the [article online](#) for updates and enhancements.

You may also like

- [Characterization of radiochromic poly\(vinyl-alcohol\)-glutaraldehyde Fricke gels for dosimetry in external x-ray radiation therapy](#)
Salvatore Gallo, Emanuele Artuso, Maria Grazia Brambilla et al.
- [A facile one-step strategy for development of a double network fibrous scaffold for nerve tissue engineering](#)
Nasim Golafshan, Hamidreza Gharibi, Mahshid Kharaziha et al.
- [Unraveling bio-inspired pre-swollen effects of tetra-polyethylene glycol double network hydrogels with ultra-stretchable yielding strain](#)
Xiaodong Wang, Haibao Lu, Nan Wu et al.

Dosimetric characterization of double network Fricke hydrogel based on PVA-GTA and phenylalanine peptide derivative

Salvatore Gallo^{1,2} , Silvia Locarno^{1,2,*} , Elisa Brambilla³ , Cristina Lenardi^{1,2} , Emanuele Pignoli⁴  and Ivan Veronese^{1,2} 

¹ Dipartimento di Fisica “Aldo Pontremoli”, Università degli Studi di Milano, via G. Celoria 16, Milano 20133, Italy

² Istituto Nazionale di Fisica Nucleare (INFN) – Sezione di Milano, Milano, Italy

³ Dipartimento di Scienze Farmaceutiche, Sezione di Chimica Generale e Organica “A. Marchesini”, Università degli Studi di Milano, via G. Venezian 21, Milano 20133, Italy

⁴ Fondazione “IRCCS Istituto Nazionale dei Tumori”, via G. Venezian 1, Milano 20133, Italy

E-mail: silvia.locarno@unimi.it

Received 7 June 2023, revised 8 September 2023

Accepted for publication 3 November 2023

Published 21 November 2023



CrossMark

Abstract

A double network hydrogel based on Poly(vinyl-alcohol) (PVA) cross-linked with Glutaraldehyde (GTA) was recently developed by using self-assembling phenylalanine (Phe) peptide derivative (Fmoc-Phe-Phe-OMe), with the aim to improve the mechanical-elastic properties of PVA-GTA hydrogels. In this study, a characterization of the properties of Xylenol Orange based Fricke gel dosimeters obtained by infusing a Fricke solution into the double network hydrogel was performed. The gel dosimeters were irradiated with 6 MV and 15 MV X-rays produced by a medical linear accelerator and investigated by means optical absorbance measurements. The double network hydrogel formulation maintained a satisfactory level of radiological water-equivalence within the investigated radiotherapy range. Fricke gel dosimeters prepared with such network kept the desired properties of independence of the response of the dose rate and energy in the investigated intervals. Furthermore, the addition of self-assembling Phe peptide derivative proved not avoid the motion of radio-induced ferric ions into the hydrogel, probably maintaining the main characteristics of the standard, no Phe peptide infused, formulation. The time course of formation of the optical response after the irradiation was observed to be similar to what previously measured in traditional PVA-GTA Fricke gel dosimeters, while a decrease of the sensitivity to radiation dose of the order of 30% was found. The extent of the decrease does not seem such as to impair the use of these dosimeters for evaluation of doses typical of radiation therapy applications. The overall dosimetric properties, coupled with the mechanical-elastic characteristics of the double network hydrogel, pave the

* Author to whom any correspondence should be addressed.



Original content from this work may be used under the terms of the [Creative Commons Attribution 4.0 licence](https://creativecommons.org/licenses/by/4.0/). Any further distribution of this work must maintain attribution to the author(s) and the title of the work, journal citation and DOI.

way to the development of phantoms able both to mimic the deformation of organs possibly occurring during radiotherapy treatments and at the same time to assess the 3D dose distribution within such volumes.

Supplementary material for this article is available [online](#)

Keywords: Fricke gel, phenylalanine peptide-derivative, double network, self-assembly, tissue equivalence, radiation dosimetry

1. Introduction

Physical phantoms, *i.e.* suitable devices which mimic human body, or a part of it, have always been indispensable tools for accurate dosimetry in external beam radiation therapy (RT). Basic dose measurements for the characterization and calibration of a RT beam are usually performed by placing a dosimeter (*e.g.* typically an ionization chamber) in a water phantom which closely approximates the radiation absorption and scattering properties of soft tissues. Solid dry phantoms, developed as substitutes for water, are also very practical devices for reference dosimetry and quality assurance (QA) measurements in RT [1].

The recent technological and procedural developments in the delivery of RT beams (*e.g.* treatments based on volumetric modulated arc therapy-VMAT or stereotactic body radiation therapy-SBRT) have also led to the development and rapid diffusion of sophisticated phantoms for patient-specific QA measurements. In general, such phantoms may integrate several active point dosimeters (*e.g.* matrixes of diodes) capable of reproducing, in the phantom, the spatial distribution of the dose absorbed by patients undergoing the RT treatment [2, 3].

In addition to homogeneous phantoms, anthropomorphic phantoms are frequently used for clinical dosimetry. Commercially available systems, evolution of the Alderson RANDO phantom [1], are shaped into a human torso and incorporate various materials to simulate different body tissues like muscles, bones, lungs and air cavities. Such phantoms are sectioned transversely into slices for dosimetric applications. Indeed, cavities in each slice allow accommodation of different types of passive point dosimeters (*e.g.* thermoluminescence dosimeters-TLDs, optically stimulated luminescence dosimeters-OSLs, alanine pellets).

A special class of phantoms that may significantly contribute to three-dimensional (3D) dose verification in complex RT procedures is represented by dosimetric phantoms. They are 3D dose integrating chemical dosimeters in which a suitable radiation sensitive chemical agent is incorporated into a hydrogel or a synthetic polymer matrix. Ideally, a dosimetric phantom can be modeled directly in an anthropomorphic shape or be inserted into an anthropomorphic phantom holder. Upon irradiation, dose-dependent changes in physical and/or optical properties of the dosimetric phantom occur as consequence of radiation induced chemical reactions. Consequently, the 3D

spatial information on the absorbed dose within the phantom can be captured and retrieved by a suitable readout technique (*e.g.* magnetic resonance imaging or optical computed tomography) [4, 5].

Various examples of dosimetric phantoms are available in the literature, most of them related to the fabrication of head phantoms containing Polymer gels or Fricke gels (FGs). They can be used for verifying the dose distribution to brain targets in stereotactic radiation therapy (SRT) procedures, as well as for performing QA end-to-end tests [6–9].

In addition to SRT treatments, an important challenge of the modern RT is still the precise delivery of the prescribed dose to targets located in, or nearby, organs subjected to motions and deformations during the RT treatment. Image-guided radiation therapy may significantly improve the precision of such treatments by using different imaging systems to reduce inter-fractional and intra-fractional motion uncertainties. The clinical implementation of motion management systems requires that they first be validated through robust tests and measurements [10, 11]. To this aim, phantoms containing dosimetric materials able not only to accurately measure 3D dose distributions, but also to mimic the deformation and motion of organs are required [12, 13]. Various deformable dosimetric phantoms have been proposed in the literature, which use different manufacturing approaches and readout techniques [14–21].

Recently, an innovative double network hydrogel based on Poly(vinyl-alcohol) (PVA) chemically cross-linked with Glutaraldehyde (GTA), was developed by the addition of self-assembling phenylalanine (Phe) derivatives. In particular, mechanical characterization measurements of the hydrogel clearly showed that the addition of the peptide Fmoc-Phe-Phe-OMe (P) produce levels of stiffness, toughness and stretchability higher than conventional PVA-GTA matrices [22]. By infusing such hydrogel with a Fricke solution, a dosimetric material was obtained, whose mechanical-elastic properties could be exploited to produce deformable dosimetric phantoms. Preliminary tests of the basic dosimetric properties of double network PVA-GTA FGs (hereinafter referred to as PVA-GTA-P FGs) were performed using ^{137}Cs as radiation source, and $^1\text{H-NMR}$ relaxometry and UV-Vis spectrophotometry as readout techniques [22].

The aim of this study is to characterize the dosimetric properties of PVA-GTA-P FGs in typical clinical RT irradiation scenarios by means of UV-Vis optical absorbance

(OA) measurements, and to compare their performances with those of traditional PVA-GTA FG dosimeters previously investigated [23–26].

2. Materials and methods

2.1. Samples preparation

PVA-GTA-P-FGs were prepared using the following materials:

Peptide Fmoc-Phe-Phe-OMe (P), whose synthesis is described in detail elsewhere [22]; PVA Kuraray Poval™18-88 (PVA-molecular weight 130 000 Da; degree of hydrolysis 86.7%–88.7%) (©Kuraray Europe GmbH [27]); GTA (solution 25% v/v in water) (Sigma-Aldrich); Xylenol Orange tetra-sodium sodium salt (XO) (Sigma-Aldrich); sulfuric acid (SA) (VWR); ferrous ammonium sulfate hexahydrate (FAS) (Carlo Erba); dimethyl sulfoxide (DMSO) (Sigma-Aldrich); Ultrapure water (resistivity 18.2 MΩ cm) obtained by a water purification system (Milli-Q Direct, EMD Millipore, Germany). All the solvents used for the PVA-GTA-P-FG preparation were of ACS grade or higher.

PVA stock solution (solution 1) was prepared by dissolving 10.6 g of PVA in 75.0 ml of ultrapure water, at 70 °C under moderate stirring (~150 rpm) for 40 min. The final concentration of PVA stock solution was 12.4% w/w. After the complete dissolution, the PVA solution was left to cool down at room temperature. Peptide solution 100 mg ml⁻¹ (solution 2) was prepared by dissolving P in DMSO by mechanical stirring for 5 min at room temperature. Fricke-XO solution (solution 3) was obtained by adding SA (25 mM), FAS (0.50 mM) and XO (0.165 mM) into water with moderate stirring (~150 rpm).

A volume of 3.7 ml of solution 2 was slowly incorporated into 112.5 g of solution 1 maintaining a rapid stirring (~400 rpm) for 2 h to reach homogeneity and clearness of the resulting PVA-P solution. Afterwards, 24.65 ml of solution 3, 9.5 ml of water and 1.35 ml of GTA solution were added and after one minute of gentle stirring, the final solution was poured for gelation into poly(methyl methacrylate) cuvettes (10 mm optical path length and 12 mm overall length) closed with polypropylene cuvette stoppers and sealed with Parafilm™.

For sake of comparison, an additional set of samples was prepared with the procedure described above and with the same amounts of reagents, including DMSO, but without the addition of peptide (hereinafter referred to as PVA-GTA-DMSO FG).

Finally, a series of Fricke-gel-layer (FGL) dosimeters with 3 mm optical path and surface dimensions 11 cm x 5 cm were prepared and used for evaluating the Fe³⁺ diffusion coefficient. Details of FGLs geometry and assembling can be found elsewhere [28].

The final concentration of PVA, DMSO and peptide in PVA-GTA-P FG dosimeters were equal to 9.11% w/w, 2.67% w/w and 0.24% w/w, respectively.

After the complete gelation, all the Fricke gel dosimeters were kept refrigerated at the controlled temperature of 6 °C for one day and brought back to room temperature one hour

before the irradiations and the subsequent optical absorbance (OA) measurements.

2.2. Radiological water-equivalence

The radiological water-equivalence of the PVA-GTA-P hydrogel was evaluated by comparing the values of density, mass energy absorption coefficients for photons and mass electronic stopping power for electrons with those of water. Furthermore, a comparison of the densities and of the interaction coefficients between PVA-GTA-P hydrogel and the previously studied PVA-GTA hydrogel [23] was performed. The PVA-GTA-P hydrogel density was measured at 25 °C by using calibrated vessels with a capillary neck and an analytical balance with precision of 0.1 mg. The uncertainty of density was obtained as the standard error of the mean value over ten different samples.

The values of mass energy absorption coefficient and mass electronic stopping power of PVA-GTA-P and PVA-GTA hydrogels were calculated as a weighted average of mass energy absorption coefficients and mass electronic stopping powers of their chemical element constituents, respectively. The chemical formulas and elemental compositions of the media of interest, reported in table 1, were used for the calculations considering the National Institute of Standards and Technology physical reference data [29].

2.3. Samples irradiation

The irradiations of the PVA-GTA-P FG dosimeters in cuvettes were carried out with 6 MV and 15 MV X-rays generated by a linear accelerator (LINAC) Varian Clinac-Trilogy (Varian Medical Systems, CA, USA) at 'Fondazione IRCCS Istituto Nazionale dei Tumori' of Milano (Italy). The LINAC was calibrated following the IAEA TRS-398 code of practice (IAEA 2000) [30].

In all experiments using 95 cm Source-surface distance, three samples, placed within a solid water slab phantom with their center at 5 cm depth, were irradiated simultaneously and uniformly using a 20 cm × 20 cm field size. Details of the irradiation geometry are available elsewhere [23].

The irradiations of the FG dosimeters in form of layers were performed using 70 kV X-rays generated by an X-rays tube (Gilardoni Radiolight, Italy). A set of three samples of FGL dosimeters was considered. During the irradiation, half of the area of each layer was partially covered with a 2 mm thick layer of lead to attenuate the beam in order to obtain a steep dose gradient. Details of the irradiation geometry are available elsewhere [31].

2.4. Optical absorbance measurements

Spectrophotometric measurements of the samples in cuvettes were performed using a Cary 100 UV-Vis spectrophotometer (Agilent Technologies, Santa Clara, CA, USA). The OA spectrum of each dosimeter in the wavelength interval 360–720 nm was collected before the irradiation, using a cuvette containing ultrapure water as reference. The same measurements were repeated approximately one hour after the irradiation of the

Table 1. Elemental compositions (% w/w) of water, GTA, PVA, SA, DMSO, Peptide and PVA-GTA-P hydrogel. Data related to the previously studied PVA-GTA hydrogel [23, 24] are also reported for sake of comparison.

Materials	Chemical formulas	w _H (%)	w _O (%)	w _N (%)	w _C (%)	w _S (%)	PVA-GTA-P hydrogels (%)	PVA-GTA hydrogels (%)
Water	H ₂ O	11.111	88.889	0.000	0.000	0.000	87.609	90.231
GTA	C ₅ H ₈ O ₂	8.000	32.000	0.000	60.000	0.000	0.234	0.241
PVA	C ₂ H ₄ O	9.091	36.364	0.000	54.545	0.000	9.114	9.386
SA	H ₂ SO ₄	2.041	65.306	0.000	0.000	32.653	0.138	0.142
DMSO	C ₂ H ₆ SO	7.693	20.513	0.000	30.769	41.025	2.663	0.000
Peptide-P	C ₃₄ H ₃₂ N ₂ O ₅	5.839	14.599	5.109	74.453	0.000	0.242	0.000
PVA-GTA-P hydrogel		10.803	81.936	0.012	6.111	1.138	100	—
PVA-GTA hydrogel		10.901	83.788	0.000	5.264	0.046	—	100

Table 2. Irradiation parameters used for the study of the dose rate dependence.

Total MU	MU rate (MU min ⁻¹)	Dose rate (cGy s ⁻¹)	Number of fractions	Time interval between fractions (s)
720	140	2.27	1	—
720	420	6.80	1	—
720	700	11.33	1	—
720	1120	18.12	1	—
720	1400	22.66	1	—
720 (6 × 120)	1400	2.25 ^a	6	56
720 (4 × 180)	1400	0.26 ^a	4	900

^a Average value over the total irradiation time.

samples. For each sample, the spectrum of the optical absorbance variation $\Delta(OA)$ (*i.e.* $OA_{\text{after irradiation}} - OA_{\text{before irradiation}}$) was accordingly derived.

A compact thermally cooled UV-VIS spectrometer (Prime X, B&WTec Inc, USA) coupled with a halogen lamp by means of silica optical fibers was initially used to measure the time-course of formation of the OA signal in one sample of PVA-GTA-P FG dosimeter in cuvette, due to the Fe^{3+} -XO complexation occurring during the first minutes after the irradiation. The same procedure previously used in the case of the study of PVA-GTA hydrogels [23] was followed. Briefly, OA spectrum of one sample, in the interval 350–700 nm, was collected before the irradiation. Afterwards, absorbance spectra were measured at consecutive times post-irradiation, starting from about 30 s up to 50 min, in 1.5 s steps.

Light transmittance images of the various FG dosimeters in form of FGLs were acquired before irradiation and at regular intervals up to 6 h post-irradiation in order to evaluate Fe^{3+} diffusion rate. A laboratory-made equipment consisting of a planar white-light illuminator (model LLUB, by PHLOX[®]) and a charge coupled device (CCD, model uEye, by IDS[®]) was employed. A narrow band-pass filter centered at 585 nm with a full width half maximum of 10 nm was placed in front of the CCD detector for selecting the spectral region of interest. Details of the equipment used for the light transmittance images of the FGL dosimeters can be found elsewhere [31].

2.5. Dosimetric characterization

The dose response and energy dependence of the PVA-GTA-P FG dosimeters in cuvette were studied by irradiating the samples at increasing doses up to 15 Gy, with 6 MV and 15 MV

x-rays in flattening filter (FF) beam mode and with 6 MV x-rays in flattening filter free (FFF) beam mode, using dose rates of 9.9 cGy s⁻¹, 10.2 cGy s⁻¹ and 11.3 cGy s⁻¹, respectively.

To evaluate the time required for the formation and stabilization of the Fe^{3+} -XO complexes within the hydrogel matrix, one PVA-GTA-P FG dosimeter in cuvette was irradiated at a dose of 8 Gy (dose rate of 9.9 cGy s⁻¹), with 6 MV-FF-x-rays, and subsequently used for measuring the time-course of the absorbance spectrum by means of the compact spectrometer (see section 2.4).

The dose rate dependence of PVA-GTA-P FG dosimeter in cuvette was studied by delivering 720 monitor units (MU) with 6 MV-FFF-x-rays, changing the MU rate from 140 to 1400 MU min⁻¹. The corresponding dose rates were in the interval 2.27–22.7 cGy s⁻¹. Furthermore, two additional tests were performed. In the first test, the total output (*i.e.* 720 MU), delivered at a rate of 1400 MU min⁻¹ was spitted in six fractions of 120 MU, spaced out at 56 s in order to reproduce an average dose rate similar to that achieved using the lowest MU rate of 140 MU min⁻¹. In the second test, the total output (*i.e.* 720 MU), delivered at a rate of 1400 MU min⁻¹ was spitted in four fractions of 180 MU, spaced out at 15 min in order to let the achievement of the chemical equilibrium of $XO-Fe^{3+}$ complexation in the samples before the subsequent irradiation fraction. Details of the irradiation parameters used to investigate the dose-rate dependence of the PVA-GTA-P FG samples are given in table 2.

2.6. Diffusion rate evaluation

The well-established procedure previously employed to evaluate Fe^{3+} diffusion rate in FG dosimeters of different compositions [25, 31] was employed. The analysis was carried

out using the light transmittance images of FGL dosimeters acquired before and after the irradiation with a steep dose gradient. For each FGL dosimeter, the differences of optical absorbance $\Delta(\text{OA})$ at 585 nm (*i.e.* in the transmittance interval of the band-pass filter) were calculated on a pixel by pixel basis and the $\Delta(\text{OA})$ profile across the steep dose gradient was derived. Fe^{3+} diffusion rate was obtained by the analysis of the temporal variation of the $\Delta(\text{OA})$ profile due to diffusion phenomena. Between the different optical measurements, the samples were kept at a controlled temperature (6 °C) and protected from light to minimize auto-oxidation. Before each measurement, the samples were thermalized at room temperature for 5 min. Details of the employed procedure for data analysis can be found in supporting information (SI).

3. Results and discussion

3.1. Radiological water-equivalence

The density of PVA-GTA-P hydrogel was assessed equal to $1.016 \pm 0.006 \text{ g cm}^{-3}$, *i.e.* similar to the value of $1.031 \pm 0.005 \text{ g cm}^{-3}$ previously obtained for PVA-GTA hydrogel [23].

Figure 1 shows the mass energy absorption coefficient *vs* photons energy for PVA-GTA-P hydrogel, compared with those of PVA-GTA hydrogel [23] and water. Similarly, figure 2 shows the mass electronic stopping power *vs* electrons energy for PVA-GTA-P and PVA-GTA hydrogels, and for water.

The addition of self-the mass electronic stopping power: the ratio of the interaction coefficient in the two gel formulations (*i.e.* PVA-GTA-P/PVA-GTA) differs from one by less than 0.5% in the whole energy range 0.01–100 MeV (see figure 2(b)). In case of photon interactions, the PVA-GTA-P hydrogel was characterized by a mass energy absorption coefficient higher than that of PVA-GTA hydrogel in the low energy region (*i.e.* below 100 keV, where the photoelectric effect is predominant). A maximum value of the ratio between the mass energy absorption coefficient of PVA-GTA-P hydrogel and of PVA-GTA hydrogel equal to about 1.11 was obtained for photon energy of approximately 30 keV (see figure 1(b)). Such difference is due to the higher concentration of sulfur in the hydrogel containing P than in conventional PVA-GTA matrices, as effect of the use of DMSO in their preparation.

In spite of this, the PVA-GTA-P hydrogel formulation maintained a satisfactory level of radiological water-equivalence, as attested by the ratios of the interaction coefficients between the hydrogel and water, whose values are close to the unit in the energy range of interest for external beam radiation therapy applications (*see* figures 1(b) and 2(b)).

Figure 3(a) shows some examples of $\Delta(\text{OA})$ spectra of one PVA-GTA-P FG sample in cuvette collected at different times, starting from 30 s up to 20 min post-irradiation (6 MV x-rays in FF mode). The time course of the $\Delta(\text{OA})$ at the wavelengths of 520 nm and 585 nm (*i.e.* the centers of the two main absorption bands) and at 555 nm (*i.e.* the isosbestic point [23]) is

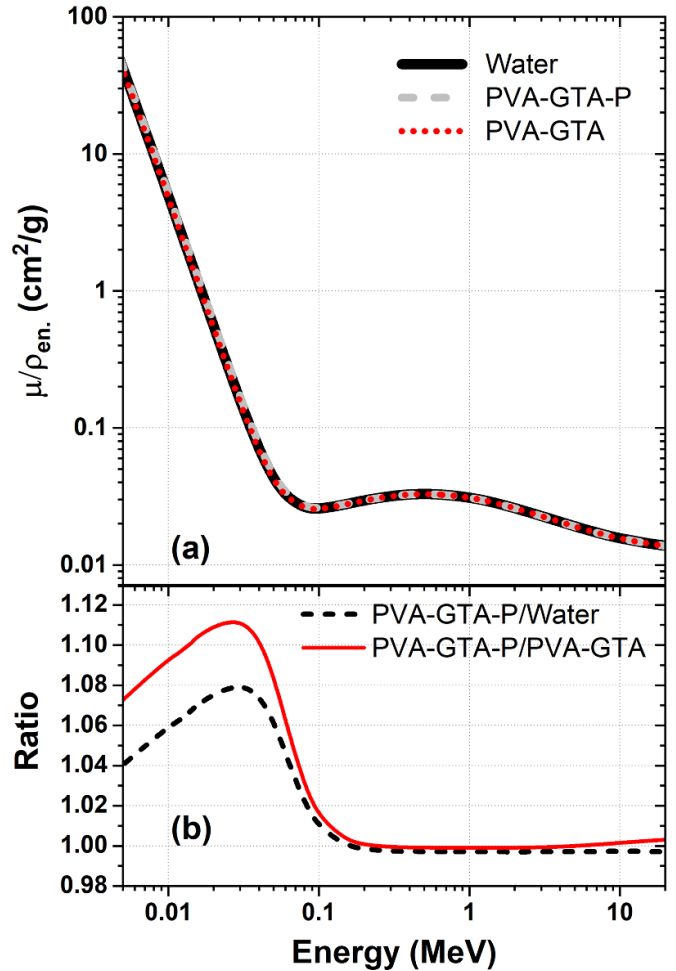


Figure 1. (a) Mass energy absorption coefficient *vs* photons energy for PVA-GTA-P hydrogel (dashed grey line), PVA-GTA hydrogel (dotted red line) and water (solid black line). (b) Ratio between mass energy absorption coefficients of PVA-GTA-P hydrogel and water (dashed black line), and ratio between mass energy absorption coefficients of PVA-GTA-P hydrogel and PVA-GTA hydrogel (solid red line). A direct comparison between PVA-GTA hydrogel and water can be found in [23].

shown in figure 3(b). The data of figure 3(b) are scaled to one considering the saturation values of the $\Delta(\text{OA})$ at the three considered wavelengths.

The results of figure 3(a) suggested that both the intensity and the shape of the $\Delta(\text{OA})$ spectrum of PVA-GTA-P FG changed with increasing the post irradiation time, *i.e.* during the phase of complexation of the radio-induced Fe^{3+} with XO. A similar behavior was previously observed in other FG dosimeters containing XO as chelating agent and can be ascribed to the dynamic of XO-Fe^{3+} complexation processes [26].

Consequently, the time intervals required to reach saturation of the $\Delta(\text{OA})$ proved to slightly depend on the wavelength, as shown in figure 3(b). However, from a practical point of view, it is reasonable to conclude that 15 min is the minimum waiting time required to stabilize the dosimetric signal in PVA-GTA-P FG dosimeters after the irradiation and

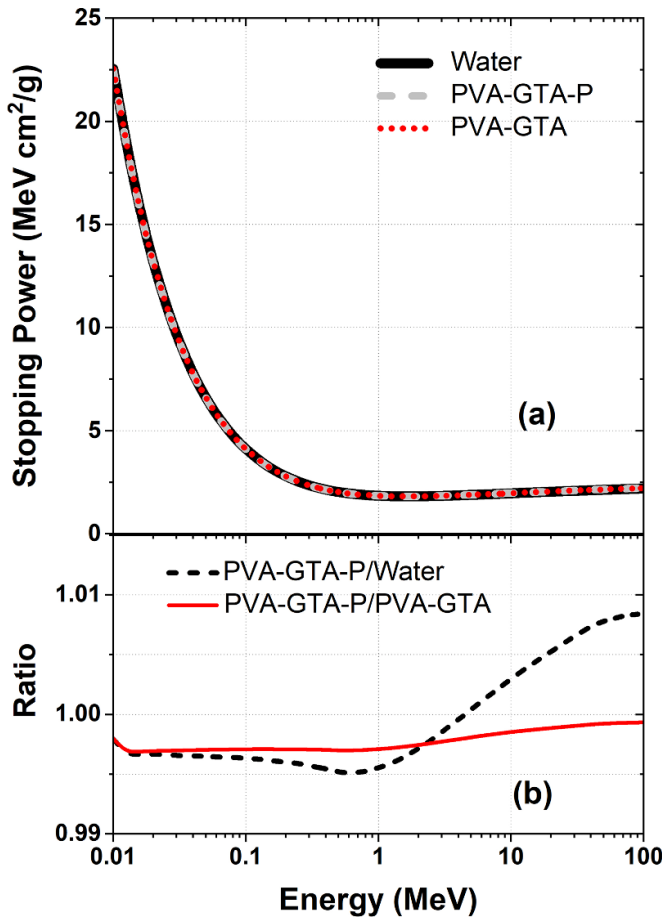


Figure 2. (a) Mass electronic stopping power vs electrons energy for PVA-GTA-P hydrogel (dashed grey line), PVA-GTA hydrogel (dotted red line), and for water (solid black line). (b) Ratio between mass electronic stopping power of PVA-GTA-P hydrogel and water (dashed black line), and ratio between mass electronic stopping power of PVA-GTA-P hydrogel and PVA-GTA hydrogel (solid red line). A direct comparison between PVA-GTA hydrogel and water can be found in [23].

before their analysis with optical techniques, independently of the wavelength used for measuring the $\Delta(OA)$.

Figure 4(a) shows examples of $\Delta(OA)$ spectra of PVA-GTA-P FG dosimeters in cuvettes, irradiated to different doses with 6 MV x-rays in FF mode. As expected, the shape of the spectra changed with increasing the dose and, most importantly, the intensity of $\Delta(OA)$ was proportional to the radiation dose. Such features were already observed in PVA-GTA-P FG prepared with different amounts of peptide and DMSO irradiated with ¹³⁷Cs sources [22]. Similar spectra were obtained in case of irradiation with 15 MV x-rays in FF mode and with 6 MV x-rays in FFF mode, as shown in the SI.

The dose-response data for the two energies (6 MV and 15 MV) and two irradiation modalities (FF and FFF), obtained by plotting the values of $\Delta(OA)$ at the wavelength of 555 nm versus the absorbed dose, are shown in figure 4(b). Linear straight lines were fitted to each set of data and the values of the slope-parameter, corresponding to dose sensitivity, together

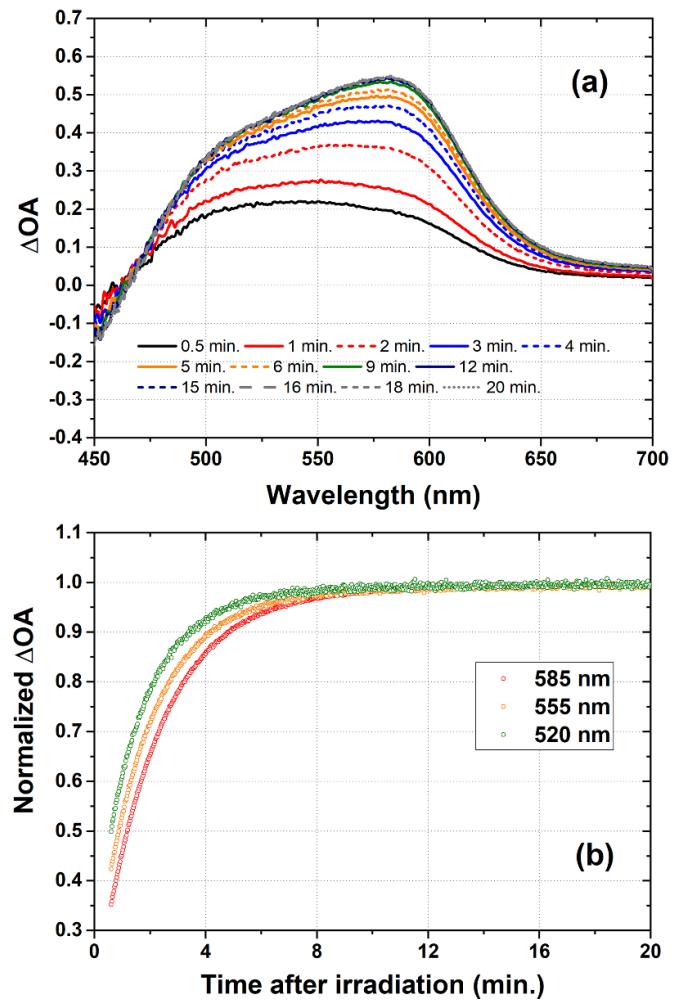


Figure 3. (a) Examples of $\Delta(OA)$ spectra of one PVA-GTA-P FG sample collected at different post-irradiation times. (b) Time course of the $\Delta(OA)$ at the wavelengths of 520 nm, 555 nm and 585 nm.

with the coefficients of determination R^2 are summarized in table 3.

It is worth noting that, as in other XO-based FG dosimeters [23], linear dose response curves over the full investigated dose interval were achieved by considering the OA variation at 555 nm, *i.e.* the isosbestic point on the $\Delta(OA)$ spectra.

The results of figure 4(b) and table 3 demonstrated that that no differences between the dose-response curves of PVA-GTA-P FG dosimeters at 6 MV (FF and FFF) and 15 MV occurred, suggesting the independence of their optical response of the energies conventionally used in x-rays radiation therapy.

The sensitivity of PVA-GTA-P FG dosimeters was slightly lower than the sensitivity previously obtained with PVA-GTA FG dosimeters [23]. This is due to the presence of DMSO in PVA-GTA-P hydrogel required to ensure solubility of P during the hydrogel preparation. In fact, it was already observed that the presence of DMSO in FG dosimeters influences their

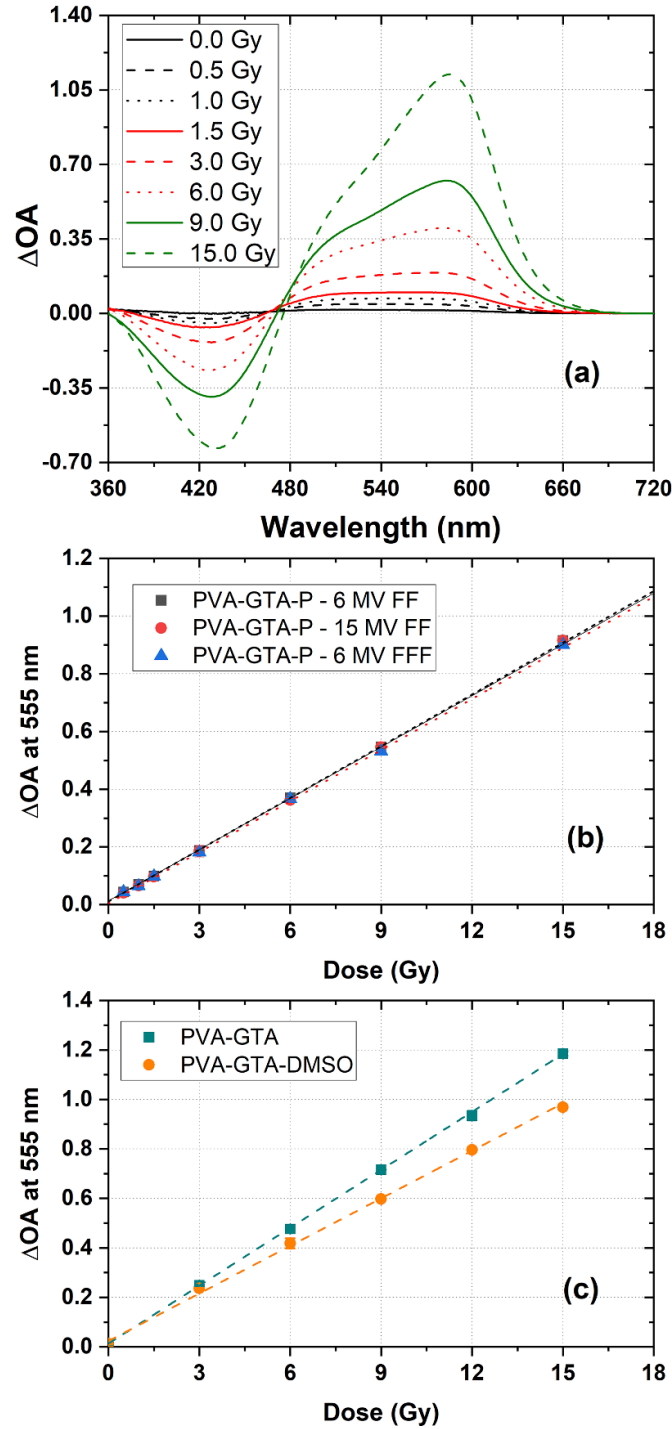


Figure 4. (a) Examples of $\Delta(OA)$ spectra of PVA-GTA-P FG dosimeters irradiated to different doses with 6 MV x-rays in FF mode. (b) Dose-response data for the two energies (6 MV and 15 MV) and two irradiation modalities (FF and FFF) obtained considering the $\Delta(OA)$ values at 555 nm. The error bars correspond to one standard deviation. The lines are the linear fits to the experimental data. (c) Dose-response data for conventional PVA-GTA FG dosimeters and PVA-GTA-DMSO FG samples irradiated to different doses with 6 MV x-rays in FF mode. The error bars correspond to one standard deviation. The lines are the linear fits to the experimental data.

dosimetric properties [22, 32, 33]. This feature is evident in figure 4(c), where the dose response data of conventional PVA-GTA FG dosimeters, irradiated with 6 MV x-rays in FF mode, are compared with those of PVA-GTA-DMSO FG samples. The sensitivity of PVA-GTA-DMSO FG samples was evaluated equal to $0.062 \pm 0.001 \text{ Gy}^{-1}$ *i.e.* similar to that

of PVA-GTA-P FG dosimeters. By contrast, the sensitivity of conventional PVA-GTA FG dosimeters results equal to $0.078 \pm 0.001 \text{ Gy}^{-1}$, *i.e.* approximately 30% higher than what achieved in PVA-GTA-P FG samples.

Examples of $\Delta(OA)$ spectra of PVA-GTA-P FG dosimeter irradiated to the same dose using different dose rates, as

Table 3. Sensitivity to radiation dose of PVA-GTA-P FG dosimeters irradiated using different energies.

Type	Sensitivity (Gy^{-1})	R-Square
PVA-GTA-P-6 MV FF	0.059 ± 0.001	0.9993
PVA-GTA-P-15 MV FF	0.060 ± 0.001	0.9996
PVA-GTA-P-6 MV FFF	0.059 ± 0.001	0.9996

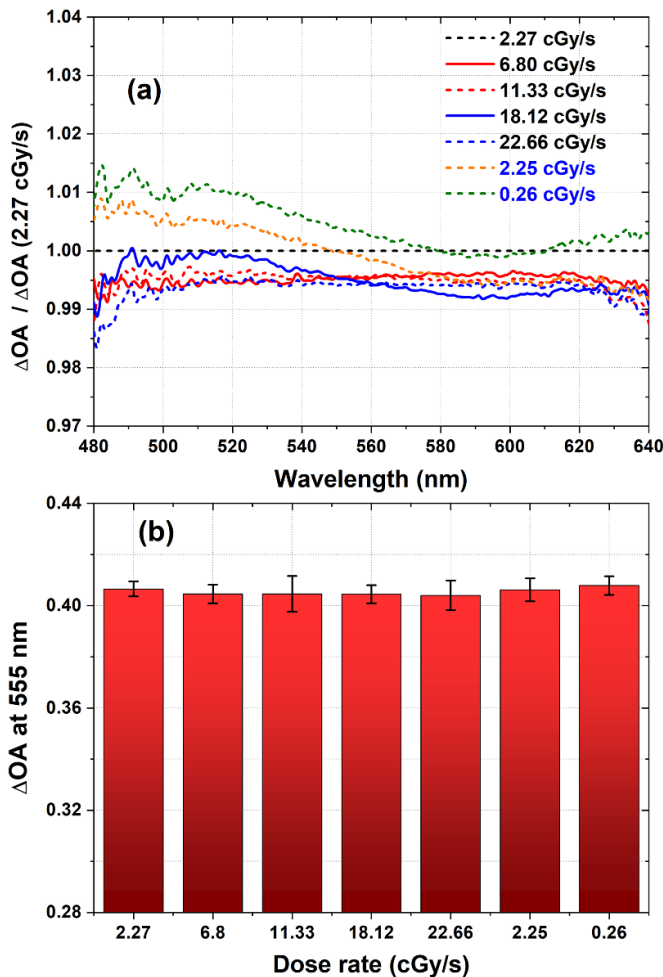


Figure 5. (a) Examples of $\Delta(\text{OA})$ spectra of PVA-GTA-P FG dosimeters irradiated to the same dose using different dose rates, normalized to the values measured at the dose rate of 2.27 cGy s^{-1} . (b) Average values of $\Delta(\text{OA})$ at the wavelength of 555 nm for the complete set of dosimeters irradiated to the same dose using different dose rates. Error bars correspond to one standard deviation.

reported in table 2, are shown in the SI (figure SI4). An overlap of the various spectra can be observed. This is also highlighted in figure 5(a) where the $\Delta(\text{OA})$ spectra, normalized to the values measured at the dose rate of 2.27 cGy s^{-1} , were plotted in the wavelength region of the main absorption peaks of Fe^{3+} -XO complexes.

Considering the $\Delta(\text{OA})$ values at the wavelength of 555 nm, shown in figure 5(b), the differences were lower than 1.0%, i.e. of the same order of magnitude of the variability observed among the samples irradiated using the same dose rates. Furthermore, the fractionation of the dose over various

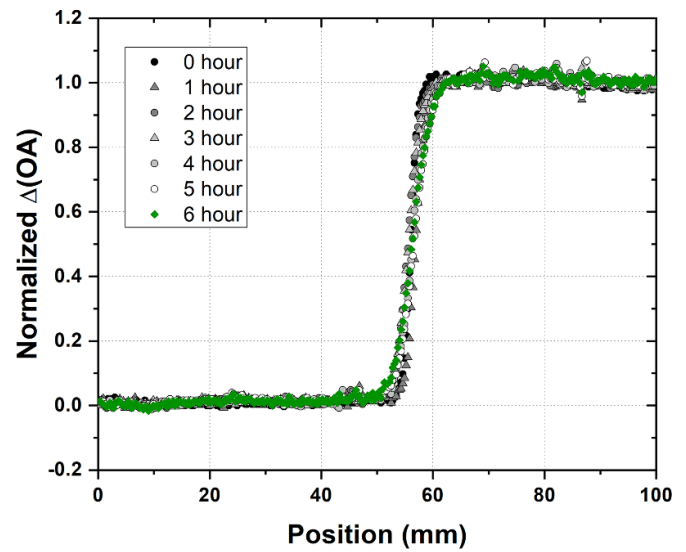


Figure 6. Examples of $\Delta(\text{OA})$ profiles in one PVA-GTA-P FG dosimeter in form of FGL, acquired at different post-irradiation times.

intervals, separated in time, had no significant effect on the final response of the dosimeter.

3.2. Diffusion rate evaluation

Figure 6 shows examples of $\Delta(\text{OA})$ profiles in one PVA-GTA-P FG dosimeter in form of FGL, acquired at different post-irradiation times. The steep dose gradient was evident, as well as its progressive smoothing due to Fe^{3+} diffusion phenomena in the hydrogel. The analysis of the temporal variation of the profile (details in the SI) revealed a diffusion coefficient equal to $0.165 \pm 0.010 \text{ mm}^2 \text{ h}^{-1}$. Such value was similar to the diffusion rate measured in various PVA-GTA FG dosimeters [25, 34–36], suggesting that the addition of P did not significantly affect the motion of radio-induced ferric ions into the hydrogel.

4. Conclusions

A characterization of the dosimetric properties of PVA-GTA-P FG dosimeters under irradiation scenarios typical of X-rays RT was performed and the results compared with those of traditional PVA-GTA FG dosimeters. The hydrogel formulation containing Phe peptide-derivative maintained a satisfactory level of radiological water-equivalence despite the higher amount of sulfur than in conventional PVA-GTA hydrogels.

The investigated PVA-GTA-P FG dosimeters proved to keep the desired properties of independence of the response of the dose rate and energy within the here investigated ranges, typical of FG dosimeters, when analyzed by means of OA measurements. Furthermore, neither a significant reduction nor an increase of the diffusion coefficient of ferric ions inside the hydrogel was observed in the PVA-GTA-P FG dosimeters, compared to what has been reported so far in the literature for other PVA-GTA FG dosimeters.

A decrease of the dose sensitivity in PVA-GTA-P FG dosimeters of approximately 30% compared to traditional PVA-GTA FG dosimeters was observed, due to the presence of DMSO in the new hydrogel formulation. However, the extent of the decrease does not seem such as to impair the use of these dosimeters for evaluation of doses typical of radiation therapy applications.

The overall dosimetric results obtained in this study, together with the outcomes of the previous investigation of the mechanical-elastic properties of the double network hydrogel, pave the way to the development of phantoms able both to mimic the deformation of organs possibly occurring during RT treatments and at the same time to assess the radiation dose distribution within such volumes.

Data availability statement

All data that support the findings of this study are included within the article (and any supplementary files).

Acknowledgments

The authors wish to thank Anna Dottor and Paola Fasano for their valid support in the hydrogel preparation. The authors are also grateful to Letizia Bonizzoni, Marco Gargano and Nicola Ludwig for their support in the irradiation of FGL dosimeters.

ORCID iDs

Salvatore Gallo  <https://orcid.org/0000-0002-5479-4577>
 Silvia Locarno  <https://orcid.org/0000-0002-1301-962X>
 Elisa Brambilla  <https://orcid.org/0000-0001-5992-4361>
 Cristina Lenardi  <https://orcid.org/0000-0002-5522-6803>
 Emanuele Pignoli  <https://orcid.org/0000-0003-3157-2135>
 Ivan Veronese  <https://orcid.org/0000-0002-3345-4303>

References

- [1] Khan F M 2019 *The Physics of Radiation Therapy* 6th edn
- [2] Urso P, Lorusso R, Marzoli L, Corletto D, Imperiale P, Pepe A and Bianchi L 2018 Practical application of Octavius[®] –4D: characteristics and criticalities for IMRT and VMAT verification *J. Appl. Clin. Med. Phys.* **19** 517–24
- [3] Srivastava R P and De Wagter C 2019 Clinical experience using Delta 4 phantom for pretreatment patient-specific quality assurance in modern radiotherapy *J. Radiother. Pract.* **18** 210–4
- [4] Marrale M and D'Errico F 2021 Hydrogels for three-dimensional ionizing-radiation dosimetry *Gels* **7** 74
- [5] De Deene Y 2022 Radiation dosimetry by use of radiosensitive hydrogels and polymers: mechanisms, state-of-the-art and perspective from 3D to 4D *Gels* **8** 599
- [6] Zirone L et al 2022 HyperArc™ dosimetric validation for multiple targets using ionization chamber and RT-100 polymer gel *Gels* **8** 481
- [7] Bry V, Saenz D, Pappas E, Kalaitzakis G, Papanikolaou N and Rasmussen K 2022 End to end comparison of surface-guided imaging versus stereoscopic X-rays for the SRS treatment of multiple metastases with a single isocenter using 3D anthropomorphic gel phantoms *J. Appl. Clin. Med. Phys.* **23** e13576
- [8] Nierer L, Kamp F, Reiner M, Corradini S, Rabe M, Dietrich O, Parodi K, Belka C, Kurz C and Landry G 2022 Evaluation of an anthropomorphic ion chamber and 3D gel dosimetry head phantom at a 0.35 T MR-linac using separate 1.5 T MR-scanners for gel readout *Z. Med. Phys.* **32** 312–25
- [9] Alexander K, Dekker K, Olding T and Schreiner L 2022 End-to-end quality assurance of stereotactic radiation therapy using an anthropomorphic head phantom *J. Phys.: Conf. Ser.* **2167** 012022
- [10] Matrosic C K, Hull J, Palmer B, Culberson W and Bednarz B 2019 Deformable abdominal phantom for the validation of real-time image guidance and deformable dose accumulation *J. Appl. Clin. Med. Phys.* **20** 122–33
- [11] Keall P J et al 2006 The management of respiratory motion in radiation oncology report of AAPM task group 76a *Med. Phys.* **33** 3874–900
- [12] Du Y, Wang R, Yue H, Zhang Y, Wu H and Wang W 2020 Dose response and stability of silicone-based deformable radiochromic dosimeters (FlexyDos3D) using spectrophotometer and flatbed scanner *Radiat. Phys. Chem.* **168** 108574
- [13] Wheatley M J, Balatinac A S, Booth J T and De Deene Y 2018 Physico-chemical properties and optimization of the deformable FlexyDos3D radiation dosimeter *Phys. Med. Biol.* **63** 215028
- [14] Matrosic C K, Bednarz B and Culberson W 2020 An improved abdominal phantom for intrafraction image guidance validation *Phys. Med. Biol.* **65** 13NT02
- [15] Matrosic C K, Culberson W, Shepard A, Jupitz S and Bednarz B 2021 3D dosimetric validation of ultrasound-guided radiotherapy with a dynamically deformable abdominal phantom *Phys. Medica* **84** 159–67
- [16] Yeo U J, Taylor M L, Dunn L, Kron T, Smith R L and Franich R D 2012 A novel methodology for 3D deformable dosimetry *Med. Phys.* **39** 2203–13
- [17] Niu C J, Foltz W D, Velec M, Moseley J L, Al-Mayah A and Brock K K 2012 A novel technique to enable experimental validation of deformable dose accumulation *Med. Phys.* **39** 765–76
- [18] Juang T, Das S, Adamovics J, Benning R and Oldham M 2013 On the need for comprehensive validation of deformable image registration, investigated with a novel 3-dimensional deformable dosimeter *Int. J. Radiat. Oncol.* **87** 414–21
- [19] Maynard E, Heath E, Hiltz M and Jirasek A 2018 Introduction of a deformable x-ray CT polymer gel dosimetry system *Phys. Med. Biol.* **63** 075014
- [20] Tajik M, Akhlaqi M M and Gholami S 2022 Advances in anthropomorphic thorax phantoms for radiotherapy: a review *Biomed. Phys. Eng. Express* **8** 052001
- [21] De Deene Y, Skyt P S, Hil R and Booth J T 2015 FlexyDos3D: a deformable anthropomorphic 3D radiation dosimeter: radiation properties *Phys. Med. Biol.* **60** 1543–63
- [22] Locarno S et al 2023 Dosimetric double network hydrogel based on poly(vinyl-alcohol)/phenylalanine-derivatives with enhanced mechanical properties *ACS Appl. Polym. Mater.* **5** 1902–14
- [23] Gallo S, Artuso E, Brambilla M G, Gambarini G, Lenardi C, Monti A F, Torresin A, Pignoli E and Veronese I 2019 Characterization of radiochromic poly(vinyl-alcohol)-glutaraldehyde Fricke gels for dosimetry in external x-ray radiation therapy *J. Phys. D: Appl. Phys.* **52** 225601
- [24] Gallo S, Lizio D, Monti A F, Veronese I, Brambilla M G, Lenardi C, Torresin A and Gambarini G 2020 Temperature behavior of radiochromic poly(vinyl-alcohol)-glutaraldehyde Fricke gel dosimeters in practice *J. Phys. D: Appl. Phys.* **53** 365003

- [25] Gallo S, Gambarini G, Veronese I, Argenti S, Gargano M, Ianni L, Lenardi C, Ludwig N, Pignoli E and d'Errico F 2019 Does the gelation temperature or the sulfuric acid concentration influence the dosimetric properties of radiochromic PVA-GTA xylenol orange Fricke gels? *Radiat. Phys. Chem.* **160** 35–40
- [26] Scotti M, Arosio P, Brambilla E, Gallo S, Lenardi C, Locarno S, Orsini F, Pignoli E, Pedicone L and Veronese I 2022 How xylenol orange and ferrous ammonium sulphate influence the dosimetric properties of PVA–GTA Fricke gel dosimeters: a spectrophotometric study *Gels* **8** 204
- [27] Kuraray Europe GmbH (available at: www.kuraray-poval.com/) (Accessed November 2023)
- [28] Gambarini G, Birattari C, Mariani M, Marchesini R, Pirola L, Prestini P, Sella M and Tomatis S 2004 Study of light transmittance from layers of Fricke-xylenol-orange-gel dosimeters *Nucl. Instrum. Methods Phys. Res. B* **213** 321–4
- [29] Hubbell J H and Seltzer S M 2004 *NIST Standard Reference Database 126* (NIST)
- [30] IAEA 2000 *IAEA TRS-398—Absorbed Dose Determination in External Beam Radiotherapy: An International Code of Practice for Dosimetry based on Standards of Absorbed Dose to Water*
- [31] Gallo S, Cremonesi L, Gambarini G, Ianni L, Lenardi C, Argenti S, Bettega D, Gargano M, Ludwig N and Veronese I 2018 Study of the effect of laponite on Fricke xylenol orange gel dosimeter by optical techniques *Sens. Actuators B* **272** 618–25
- [32] Jin C, Chen J, Yang L, Luo W, Wu G and Zha Y 2012 Effect of DMSO on the sensitivity and diffusion of FPGX gel dosimeter *Radiat. Phys. Chem.* **81** 879–83
- [33] Rabaeh K A, Eyadeh M M, Hailat T F, Madas B G, Aldweri F M, Almomani A M and Awad S I 2021 Improvement on the performance of chemically cross-linked fricke methylthymol-blue radiochromic gel dosimeter by addition of dimethyl sulfoxide *Radiat. Meas.* **141** 106540
- [34] Marini A, Lazzeri L, Cascone M G, Ciolini R, Tana L and d'Errico F 2017 Fricke gel dosimeters with low-diffusion and high-sensitivity based on a chemically cross-linked PVA matrix *Radiat. Meas.* **106** 618–21
- [35] Marralle M, Collura G, Gallo S, Nici S, Tranchina L, Abbate B F, Marineo S, Caracappa S and D'Errico F 2017 Analysis of spatial diffusion of ferric ions in PVA-GTA gel dosimeters through magnetic resonance imaging *Nucl. Instrum. Methods Phys. Res. B* **396** 50–55
- [36] Lazzeri L, Marini A, Cascone M G and D'Errico F 2019 Dosimetric and chemical characteristics of Fricke gels based on PVA matrices cross-linked with glutaraldehyde *Phys. Med. Biol.* **64** 085015